05

Theoretical study of the influence of parameters of the amplifying and absorbing media on the dynamics of coherent mode locking in a two-section laser

© R.M. Arkhipov¹, M.V. Arkhipov¹, O.O. Diachkova^{1,2}, A.V. Pakhomov^{1,2}, N.N. Rosanov¹

e-mail: arkhipovrostislav@gmail.com, mikhail.v.arkhipov@gmail.com, o.o.dyachkova@gmail.com, antpakhom@gmail.com, nnrosanov@mail.ru

Received April 15, 2025 Revised April 28, 2025 Accepted April 29, 2025

A theoretical study of the influence of the parameters of the amplifying and absorbing media on the dynamics of coherent mode locking (CML) in a two-section laser is carried out. Based on analytical calculations and numerical modeling, the conditions for the formation of a stable CML regime with parameters characteristic of terahertz quantum cascade lasers (QCLs) are studied. Using the generalized area theorem, the existence and stability of the CML regime in such systems are proven. Numerical solution of nonlinear equations describing the interaction of radiation with the active and passive media made it possible to determine the key parameters affecting the CML dynamics. It is shown that the ratio of population relaxation times in the amplifying and absorbing media plays a critical role. The obtained results are important for the development of self-starting compact laser systems generating short pulses, in particular, for terahertz QCLs. Such systems are promising for use in ultrafast spectroscopy and other applications requiring stable generation of ultrashort pulses.

Keywords: coherent mode locking, two-section laser, quantum cascade laser, self-induced transparency, nonlinear dynamics.

DOI: 10.61011/EOS.2025.06.61663.7912-25

1. Introduction

Coherent Mode Locking (CML), theoretically predicted more than 30 years ago [1], represents a mechanism for generating short pulses in a two-section laser based on the formation of 2π self-induced transparency (SIT) pulses in the absorbing medium [2,3]. This type of synchronization arises from the coherent interaction of laser radiation with the medium when the pulse duration becomes shorter than the polarization relaxation time T_2 in both the amplifier and the absorber [4–8]. Unlike standard passive mode-locking, which is implemented through incoherent saturation of gain and absorption [9,10], the CML regime allows overcoming the pulse duration limit imposed by time T_2 and achieving pulse generation as short as a single oscillation cycle in lasers with an ultrashort resonator [7].

Active theoretical studies of CML in two-section lasers have only begun recently [4–8,11–13]. In [6] and subsequent works [11,12], an analytical approach to describing CML based on the McCall-Hahn area theorem was developed. Experimentally, the CML regime was first realized in a titanium-sapphire laser with a coherent absorber [13]. CML is considered a promising mechanism for generating short pulses in quantum cascade lasers (QCLs) [4,8], where standard passive mode-locking is challenging due to extremely fast relaxation times [14–17].

However, existing theoretical works on CML in QCLs [4,8] use practically difficult schemes that do not allow self-starting of generation. In [18] passive mode-locking was experimentally demonstrated in a terahertz solid-state laser with a graphene saturable absorber, but this regime was also incoherent. From a practical point of view, CML has significant advantages, enabling the generation of shorter and more powerful pulses compared to standard passive mode-locking [19]. In [20] the possibility of self-starting CML in the IR and THz ranges was theoretically shown in lasers with fast relaxation times under parameters close to those realizable in QCLs. Nevertheless, a detailed study of the influence of system parameters on CML dynamics under such conditions is still lacking.

In this work, which is a follow-up of [20], our goal is to systematically study how the laser system parameters affect the feasibility of CML implementation. In particular, we examine the influence of two key ratios:

- The ratio of polarization relaxation time to population difference relaxation time T_2/T_1 ;
- The ratio of dipole moments of the absorber and amplifier d_a/d_g on output radiation characteristics such as pulse duration, maximum amplitude, and generation type.

To study the dependence of main characteristics of the CML regime on laser parameters, an analytical approach based on the area theorem was also used. Specifically, dependencies on parameters such as pumping level, res-

¹ loffe Institute, St. Petersburg, Russia

² St. Petersburg State University, St. Petersburg, Russia

onator's round-trip time, relaxation times in the active medium, and the ratio of transition dipole moments in the absorber and amplifier were considered.

This paper is organized as follows: Section 2 presents the theoretical model and discusses the parameters used; Section 3 studies the influence of laser system parameters on CML feasibility based on three cases leading to femtosecond pulse generation. Section 4 is devoted to the analytical description of coherent propagation of ultrashort pulses in a resonant medium based on the area theorem; the dynamics of the initial pulse area change as it propagates in the resonator during parameter variation are studied. Using this approach, questions about the existence and stability of CML regime with varying resonator and medium parameters in both laser sections were investigated.

2. Theoretical model

In this work, as in [20], a two-section laser model placed in a ring resonator with unidirectional generation mode was used; the scheme is shown in Fig. 1, a. The absorbing and amplifying media were modeled in the two-level approximation, assuming homogeneous broadening of the transition. Mirrors 1, 3 and 4 were fully reflecting, and mirror 2 had reflection coefficient: $R_{\text{resonator}} = 0.8$.

Numerical calculations were performed by solving the Maxwell-Bloch equations system for the slowly varying amplitude of the electric field A(z,t) the slowly varying polarization amplitude — the imaginary part of the off-diagonal element of the two-level density matrix $P_s(z,t)$ and the population difference of the two-level medium. This system of equations has the following form [2,20]:

$$\frac{\partial}{\partial t} A_{a,g}(z,t) + \frac{\partial}{\partial z} A_{a,g}(z,t) = 4\pi \omega_0 d_{12_{a,g}} N_{0_{a,g}} P_{s_{a,g}}(z,t),$$

$$\frac{d}{dt} P_{s_{a,g}} = -\frac{P_{s_{a,g}}(z,t)}{T_{2_{a,g}}} + \frac{d_{12_{a,g}}}{2\hbar} n_{a,g}(z,t) A_{s_{a,g}}(z,t),$$

$$\frac{d}{dt} n_{a,g}(z,t) = -\frac{n_{a,g}(z,t) - n_{0_{a,g}}}{T_{1_{a,g}}} - \frac{2d_{12_{a,g}}}{\hbar} A_{s_{a,g}}(z,t) P_{s_{a,g}}(z,t).$$
(3)

In numerical simulations, CML generation was started from a constant electric field strength in the resonator, with magnitude 10^{-13} (in CGSE units). All mirrors 1, 3, 4 were fully reflective; mirror 2 had reflection coefficient R. Initial polarization $P_{s_{a,g}}(z,0)=0$ in all media and initial inversion values $n_{0a}=1$, $n_{0g}=-1$ were set.

Here and onward, the indices a and g correspond to absorber and gain media, respectively. T_1 is the population difference relaxation time, T_2 is the polarization relaxation time, d_{12} is the transition dipole moment, n_0 is the equilibrium value of the population difference ($n_{0a} = 1$,

 $n_{0g}=-1$), N_0 is the particle concentration, ω_0 is the resonance transition frequency (same for gain and absorber). Zero detuning ($\Delta\omega=0$) and homogeneous broadening of the resonant transition is assumed. Parameters used in numerical calculations are shown in the table. For both gain and absorber media, all parameters were equal except for the medium length (the length ratio of absorber L_a to gain section L_g was set as 1:3) and the transition dipole moment. Experimental results show that coherent pulse propagation and Rabi oscillations are realizable in QCLs and can be described using few-level medium models with Maxwell-Bloch type equations (1)-(3) [21].

3. Numerical Simulation Results

To investigate pulse generation dependence on media parameters in the resonator, numerical solutions of Maxwell-Bloch equations (1)–(3) were carried out for each parameter set. After many resonator round-trips, it was either established that no generation occurred or parameters of generated pulses were measured: full-width at half maximum (FWHM) (*FWHM*, fs), maximum electric field $|A(z)|^2$ (*Pulse amplitude, arb. units*) and interval between adjacent pulses Δ ; These were averaged over many pulses ($N \sim 200$).

For illustration, Fig. 1,b-e shows the results of the numerical solution of system (1)-(3) for one set of parameters: case 2 in the table, the ratio of the relaxation times of polarization and the population difference, $T_2/T_1=0.2$, $T_2=2\,\mathrm{ps}$. Fig. 1,b and 1,e display intensity vs. time and the generation spectrum, respectively. Additionally, in the steady state regime, a segment of the intensity time dependence showing two single pulses is given (Fig. 1,c), as well as the instantaneous spatial distribution of the electric field amplitude $|A(z)|^2$, the population difference $\Delta\rho(z)$ and polarization amplitude Ps(z) as the pulse passes through the amplifier section (Fig. 1,d).

For most of the parameter sets considered below, as well as for the case shown in Fig. 1, b, after a stabilization period (on average about 500 ps), the generation consists of a sequence of identical short pulses following each other at a constant interval Δ indicating that the mode locking has been achieved. In each case, the FWHM-pulse duration is shorter than the polarization relaxation time T_2 ; satisfying this condition is necessary to consider the mode synchronization coherent. Note also that, as seen in Fig. 1, e, the resulting spectrum is significantly broader than the Lorentzian homogeneous broadening contour, which is characteristic exclusively of coherent mode locking.

The pulse roundtrip time in the resonator $T_{\rm rt}$) for this configuration is $\sim 10\,{\rm ps}$, and unless otherwise specified, the interval between pulses was $\Delta=T_{\rm rt}$, indicating a single-pulse regime.

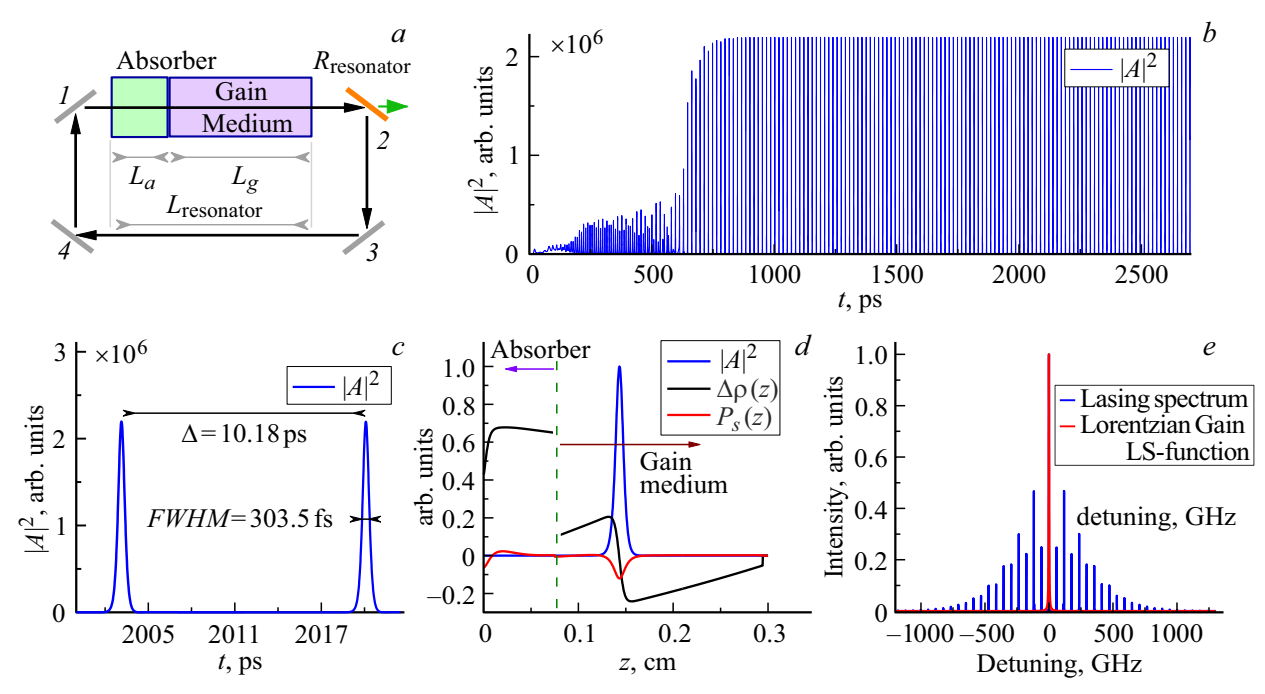


Figure 1. (a) Diagram of a two-section laser with a ring resonator containing an amplifying and an absorbing medium; 1, 2, 3, 4—resonator mirrors. (b) Dependence of the square of the electric field amplitude $|A(z)|^2$ (generation intensity) on time at the resonator output, (c) two single generation pulses and some of their parameters; (d) distribution of the electric field amplitude $|A(z)|^2$ in the resonator (blue line), population difference $\Delta \rho(z)$ (black line) and Ps(z) during the pulse passing through the amplifier section. (e) Generation spectrum (blue line) and Lorentzian gain line contour (red line).

Table.				
Parameter	Description	1	2	3
Absorber	Detuning, rad/s d , D (ESU, 10^{-18}) T_1 , ps T_2 , ps n , cm ⁻³	0 10 10 4 5.00E+16	0 10 20 7 5.00E+16	0 14 10 4 5.00E+16
Gain	Detuning, rad/s d , D (ESU, 10^{-18}) T_1 , ps T_2 , ps n , cm ⁻³	0 5 10 4 5.00E+16	0 5 20 7 5.00E+16	0 7 10 4 5.00E+16
Resonator	$\lambda,\mu{ m m}$ $L_{ m resonator},{ m cm}$	14 0.3	14 0.3	14 0.3

0.8

Table.

Note. Initial parameters used in calculations; values that were varied are italicized.

 $R_{\rm resonator}$

3.1. Dependence of Generation Parameters on the Ratio of Polarization and Population Difference Relaxation Times T_2/T_1

Since the polarization relaxation time T_2 depends on the device's operating temperature, temperature fluctuations of the resonator can lead to changes in pulse duration or even generation failure. Therefore, we examined the dependence of generated pulse parameters on the ratio of polarization relaxation time to population difference relaxation time T_2/T_1 .

Two cases were considered ($T_1 = 10 \text{ ps}$ and $T_1 = 20 \text{ ps}$, see parameter sets 1 and 2 in the table), where, with all other parameters fixed, time T_2 was varied for both absorber and amplifier.

0.8

Fig. 2 shows the dependence of FWHM and pulse amplitude on the ratio T_2/T_1 . For both cases, in the interval $0.1 < T_2/T_1 < 0.6$ there is a clear hyperbolic dependence of both pulse width and amplitude on T_2 ; as T_2 increases, the single pulse duration decreases while its amplitude increases.

0.8

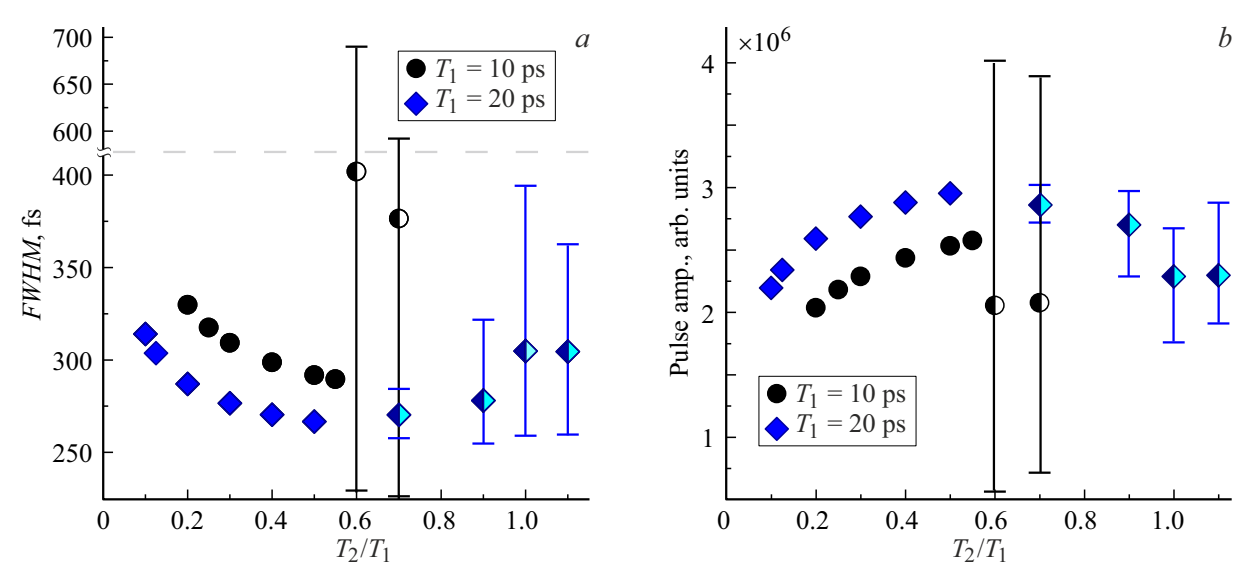


Figure 2. Dependence on the ratio T_2/T_1 (a) pulse full-width at half-maximum (FWHM) and (b) maximum electric field amplitude $|A(z)|^2$ circles correspond to $T_1 = 10$ ps, diamonds to $T_1 = 20$ ps. Cases of generation with varying pulse forms are marked by half-filled symbols, with horizontal lines indicating the maximal and minimal FWHM and amplitude values.

After $T_2/T_1 > 0.6$ the generation type changes abruptly — generated pulses now have varying maximum intensity and duration. These cases are indicated on Fig. 2 with half-filled symbols, showing the range of *FWHM* and amplitude. An example of generating varied pulses for $T_1 = 20 \,\mathrm{ps}, \, T_2/T_1 = 1$ is presented in Fig. 3, a. It is seen that although the interval between pulses Δ is maintained, other pulse characteristics vary from pulse to pulse.

The dependence of the interval between pulses Δ on the ratio T_2/T_1 is shown in Fig. 4, a. As above, cases with different pulse shapes are marked by half-filled symbols. As seen in Fig. 4, a, even in cases of varying pulse forms for $T_1=20\,\mathrm{ps}$ generation was always single-pulse ($\Delta=T_{\mathrm{rt}}\sim10\,\mathrm{ps}$). For $T_1=10\,$ ps the generation regime was dual-pulse ($\Delta=0.5T_{\mathrm{rt}}\sim5\,\mathrm{ps}$) except for two cases: although the average Δ was about $0.5T_{\mathrm{rt}}$, the interval between pulses varied, with maximum and minimum values indicated by horizontal lines in the graph.

For $T_1 = 10$ ps compared to $T_1 = 20$ ps the spread of amplitudes and pulse widths is much greater. For the $T_1 = 10$ ps case, pulse generation ceased at $T_2/T_1 < 0.2$ and $T_2/T_1 > 0.7$, whereas for $T_1 = 20$ ps generation was possible over a wider range $(0.1 < T_2/T_1 < 1.1)$. All this indicates greater stability for the $T_1 = 20$ ps case and a wider potential application range.

As already noted, polarization relaxation time T_2 depends on operating temperature. The above results suggest that for the initial parameter sets considered here (table), small changes in T_2 do not alter pulse generation character (single pulse period, identical pulse shapes). We also demonstrated the existence of a stable interval $0.1 < T_2/T_1 < 0.6$, where increasing T_2 simultaneously allows increasing pulse amplitude by about 30% and shortening pulse duration

 $(330 \rightarrow 290 \text{ fs} \text{ for } T_1 = 10 \text{ ps} \text{ case and } 305 \rightarrow 260 \text{ fs} \text{ for } T_1 = 20 \text{ ps case}).$

3.2. Dependence of Generation Parameters on the Ratio of Dipole Moments of Absorber and Amplifier d_a/d_g

Now consider the dependence of generated pulse characteristics on the ratio of dipole moments in the absorber and amplifier d_a/d_g . The dipole moment of the radiative transition in a quantum cascade laser depends on the applied electric field (or bias voltage), which thus opens the possibility of tuning generation parameters without changing the resonator cell. Two cases were studied ($d_g = 5D$ and $d_g = 7D$, see sets 1 and 3 in the table); with all other parameters fixed, the dipole moment of the absorber d_a was varied.

Let us focus on the interval between generated pulses. The dependence of the pulse separation Δ on the ratio d_a/d_g is shown in Fig. 4, b. As seen, in most cases the pulse interval was $\Delta=0.5T_{\rm rt}$ indicating a dual-pulse regime. Only in two cases ($d_g=5D$, $d_a/d_g=3$ and $d_a/d_g=4.6$) was the regime single-pulse, i.e., $\Delta=T_{\rm rt}=10$ ps. There were also regimes with non-constant pulse intervals: for several values $d_g=5D$, $3< d_a/d_g<4.5$ intensities, pulse widths (Fig. 5), and intervals ($\Delta\sim0.5-5$ ps, $\Delta_{\rm mean}\sim3.33$ ps= $T_{\rm rt}/3$)varied. In two cases, for $d_g=7D$ at $d_a=9D$ and $d_a=10D$, generation of identical and different pulses with constant interval $\Delta=3.33$ s= $T_{\rm rt}/3$ occurred. In a separate case with values $d_g=7D$, $d_a=8D$, $d_a/d_g=1.143$, stable generation of identical pulses with repetition period was observed. $\Delta=2.5$ ps= $T_{\rm rt}/4$.

Fig. 5 shows the dependence of FWHM and pulse amplitude on the ratio d_a/d_g . For both cases, there

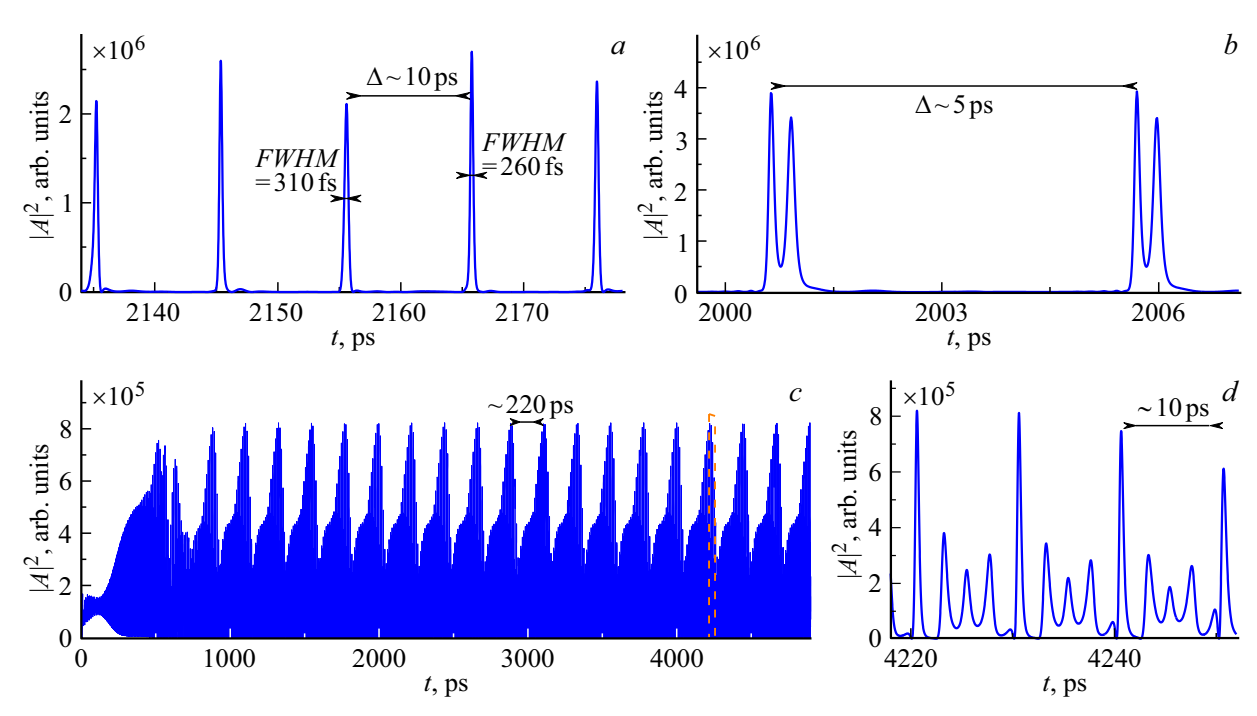


Figure 3. (a) Several single generation pulses and some of their parameters for case 2, $T_1 = T_2 = 20$ ps. (b) Two single pulses for case 1, $d_a = 5D$, $d_a/d_g = 4.8$. (c) Dependence of the square of the electric field amplitude $|A(z)|^2$ on time at the resonator output for case 3, $d_a = 7D$, $d_ad_g = 1$ with an enlarged inset (orange hatching). (d) Several single pulses and some parameters.

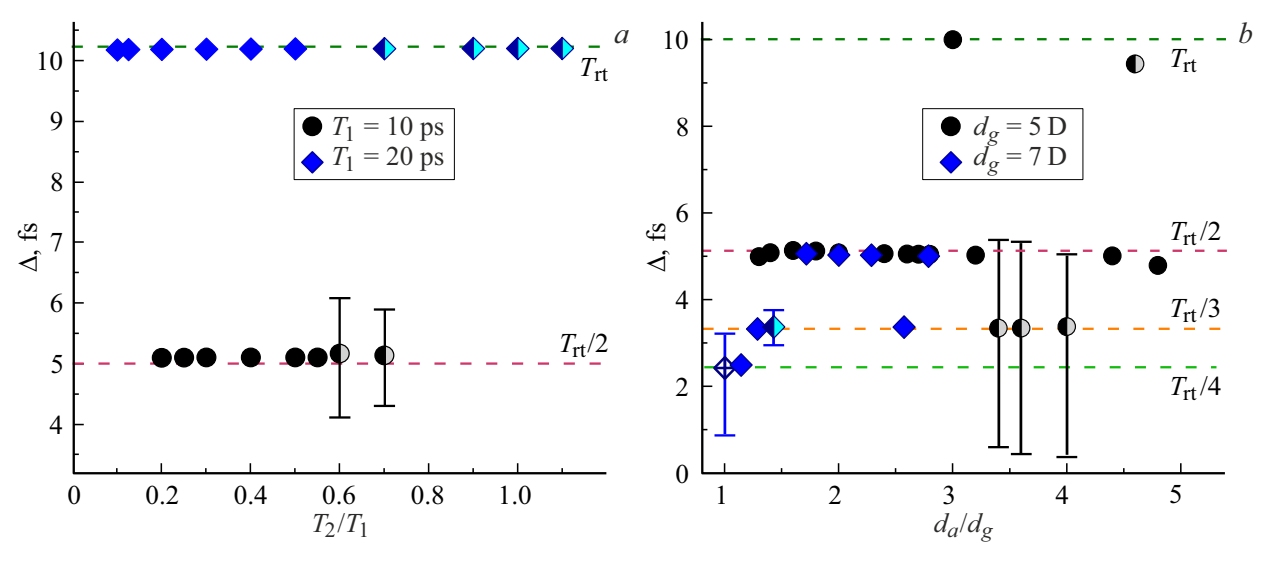


Figure 4. Dependence of the interval between pulses $\Delta(a)$ on ratio T_2/T_1 (b) and ratio d_a/d_g . Cases with generation of pulses of varying forms are marked by half-filled symbols with horizontal lines showing maximal and minimal values.

is again a hyperbolic dependence of pulse width and amplitude on d_a . Specifically, increasing d_a results in shorter single pulses and higher amplitude pulses. For the $d_g=5D$ case, the generation range was $1.2 < d_a/d_g < 5$, although the generation character changed after $d_a/d_g > 3$. The values for which coherent generation started with a large delay (more than 5 ns, or 500 resonator round-trips) are marked on Fig. 5, a by a green hatched rectangle. Additionally, pulses for $d_a/d_g > 4.5$ (marked

by a gray rectangle on Fig. 5, a) were double-peaked; an example of two such separate pulses for $d_a = 5D$, $d_a/d_g = 4.8$ is given in Fig. 3, c. The generation mode was dual-pulse ($\Delta = 0.5T_{\rm rt} \sim 5\,{\rm ps}$), and if each peak is considered separately, as seen in Fig. 5, a, they have the minimal pulse width ($FWHM \sim 100-60\,{\rm fs}$) for this dipole moment value. Considering the group of two pulses together, their combined width is $\sim 350\,{\rm fs}$.

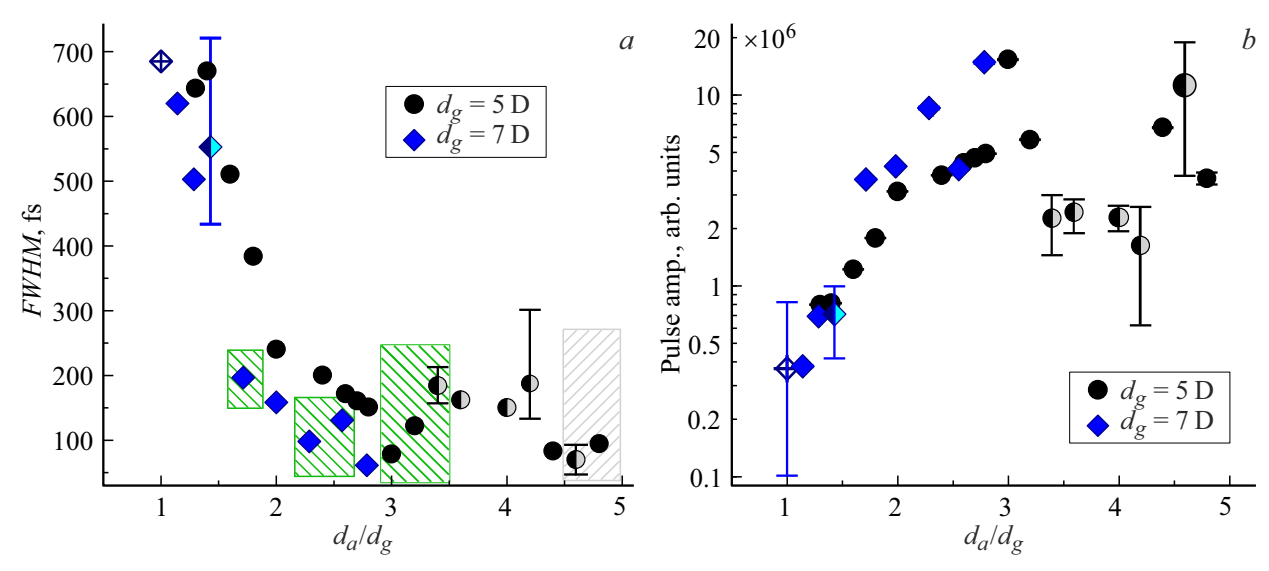


Figure 5. Dependence on the ratio d_a/d_g (a) pulse full-width at half-maximum (FWHM) (b) maximum electric field amplitude $|A(z)|^2$ black circles correspond to $d_g = 5D$, blue diamonds to $d_g = 7D$. Cases of varying pulse shapes are marked by half-filled symbols, with horizontal lines indicating max and min FWHM and amplitude.

For one parameter set, $d_g = 7D$, $d_a/d_g = 1$ (marked on Fig. 5 by a diamond with a cross), generation was observed in a,,pulsed" regime; the dependence of the square of the electric field amplitude $|A(z)|^2$ on time at the resonator output and an enlarged fragment showing several single pulses are presented in Fig. 3, c and 3, d respectively. As can be seen, for this case there is a large envelope period of $|A(z)|^2$ on the order of 220 ps, as well as a small repetition period of about $T_{\rm rt} \sim 10$ ps. The pulses vary significantly in both amplitude and width, but the generation remains stable over the relatively long period.

For the case $d_g = 7D$ the generation range was significantly smaller, $1 < d_a./_g < 2.8$. We note the case $d_a = 19.5D$, $d_a/d_g \cong 2.79$, where the generation of the largest amplitude pulses $(|A(z)|_{\max}^2 \sim 1.5 \cdot 10^7 \, \text{ESU})$ and simultaneously the shortest pulses $(FWHM = 60 \, \text{fs})$ was achieved.

Thus, we observe the existence of generation over a wide range of values of d_a . For the $d_g=7D$ case, although a clear dependence of generation parameters on the ratio of dipole moments d_a/d_g is observed, it is difficult to identify stable regions. As seen in Fig. 4, b and Fig. 5, increasing d_a changes the generation regime — two-pulse, three-pulse, and four-pulse regimes are possible.

For $d_g=5D$ we can point to the existence of a stable region $1.2 < d_a/d_g < 3$, in which increasing d_a allows simultaneously a substantial increase in pulse amplitude (\sim by a factor of 3) and reduction in pulse duration $(670 \rightarrow 160 \, \mathrm{fs})$, while maintaining stable generation with a constant repetition period ($\Delta=0.5T_{\rm rt}$) and identical pulse shapes.

Analysis of CML Using the Area Theorem

Direct numerical modeling of laser dynamics allows clear tracing of the establishment of a steady-state generation regime at given laser system parameters. At the same time, investigating the dependence of laser generation on various medium or resonator parameters proves complicated because partial differential equations must be solved for each parameter set. Therefore, for such tasks, analytic models describing the laser nonlinear dynamics are more convenient.

The most suitable analytic method for describing coherent propagation of ultrashort pulses in resonant media is based on the so-called area theorem [2,3]. Within this approach, instead of solving equations for the electric field E(z,t) the change in a quantity called the pulse area, defined as

$$\Phi(z) = \frac{d_{12}}{\hbar} \int_{-\infty}^{+\infty} E(z, t) dt, \tag{4}$$

where d_{12} is the dipole moment of the resonant transition in the medium, and, \hbar is the reduced Planck constant. The change in pulse area $\Phi(z)$ along the propagation coordinate for an ultrashort pulse in a resonant medium with strong inhomogeneous line broadening is described by a simple differential equation known as the area theorem:

$$\frac{d\Phi(z)}{dz} = \alpha n_0 \sin \Phi(z),\tag{5}$$

where α is the gain coefficient dependent on medium properties, and, n_0 is the population inversion in the

medium. The area theorem (2) admits an explicit analytic solution:

$$\operatorname{tg} \frac{\Phi(z)}{2} = e^{\alpha n_0 z} \operatorname{tg} \frac{\Phi_0}{2}. \tag{6}$$

Although the area theorem (5), (6) does not allow direct investigation of the electric field dynamics, its analytic accessibility makes it very convenient for exploring the dependence of fundamental laser dynamic characteristics on various parameters.

The standard area theorem in the form (5) was derived for a single pass of an ultrashort pulse through the medium. However, in a laser, the pulse propagates within the resonator and repeatedly returns to the medium after each round-trip. For this case, the standard area theorem (5) becomes inapplicable. A corresponding generalization of the area theorem (5), taking into account pulse propagation in medium placed in a ring resonator, was recently derived in works [11,12] and has the form:

$$\begin{split} \frac{d\Phi_{k+1}(z)}{dz} &= \alpha \bigg(n_k(z) \sin \Phi_{k+1}(z) \\ &- \frac{P_k(z)}{d_{12}} \sin^2 \frac{\Phi_{k+1}(z)}{2} \bigg), \quad 0 \le z \le L, \quad (7) \\ n_{k+1}(z) &= \bigg(n_k(z) \cos \Phi_{k+1}(z) \\ &- \frac{P_k(z)}{d_{12}} \sin \Phi_{k+1}(z) \bigg) e^{-T_{rt}/T_1} + n_0 (1 - e^{-T_{rt}/T_1}), \\ P_{k+1}(z) &= (P_k(z) \cos \Phi_{k+1}(z) \\ &+ d_{12}n_k(z) \sin \Phi_{k+1}(z)) e^{-T_{rt}/T_2}, \end{split}$$

where function $\Phi k(z)$ defines the pulse area (4) at the k-th round-trip iteration, $n_k(z)$ and $P_k(z)$ represent the population inversion and induced polarization of the resonant medium at coordinate z respectively after k full resonator round-trips,L is the length of the medium layer. The spatial coordinate z is measured along the direction of pulse propagation along the resonator axis throughout the resonant medium layer. Boundary conditions linking the pulse area values at two successive round-trips are determined by reflection of the pulse at the output mirror with amplitude reflection coefficient r:

$$\Phi_{k+1}(z=0) = r\Phi_k(z=L).$$

In the case of a two-section laser, the system of equations (7) must be solved separately at each resonator round-trip iteration for pulse propagation in the amplifier section and separately for the absorber section. Accordingly, all parameters for both media can be different. For simplicity, below we use the same relaxation times T_1 and T_2 for both media but vary the transition dipole moments d_{12} and coefficients α independently for both. As before, parameters related to the gain and absorber media are denoted by subscripts g or a respectively.

Let us first consider the optimal case where the dipole moment of the resonant transition in the absorber is twice that in the amplifier. In this case, a stable 2π -pulse in the absorber simultaneously represents a stable π -pulse in the amplifier. The dynamics of the initial pulse area as it propagates in the resonator were studied using system The number of resonator round-trip iterations in (7) was chosen such that the system reached a steady state. Calculations showed that throughout the considered parameter range, system (7) describes convergence to stable stationary values when starting from initial zero induced polarization in the medium, equilibrium values $n_{0,g}$ and $n_{0,a}$ for population inversion, and a small seed for the initial pulse area $\Phi_1(0) \ll \pi$. No periodic or more complex nonperiodic dynamic regimes of system (7) were found. Thus, one can conclude the existence and stability of the coherent mode synchronization regime in the studied laser system.

Fig. 6, a, b shows results from the generalized area theorem (7) calculations for dipole moment ratio $m_d = d_a/d_g = 2$ and other parameters from the previous section. The varied parameters are the ratio of relaxation times $T_{\rm rt}/T_1$ and the dimensionless pump level in the amplifier $\alpha_g n_{0,g} L_g$. Fig. 6, a shows stationary values of the pulse area at the absorber section output, Fig. 6, b the steady-state pulse area at the amplifier section output. From these figures, above a certain generation threshold, a stable CML regime is established with pulse area values smaller than the corresponding stable values in an infinite medium, namely π in the amplifier and 2π in the absorber. Meanwhile, pulse area values on Fig. 6, a, b tend to approach π in the amplifier and 2π in the absorber in the limit of large pump excess above threshold and very fast population inversion relaxation $T_{\rm rt}/T_1 \gg 1$.

Fig. 7, a and 7, b shows the corresponding steady-state values of the population inversion in both laser sections for the same parameter ranges as in Fig. 6, a and 6, b. It is evident that the population inversion approaches its equilibrium values in the case of very fast inversion relaxation $T_{\rm rt}/T_1 \gg 1$. Conversely, for sufficiently slow inversion relaxation relative to the resonator round-trip time, the inversion tends toward zero in absolute value. This result can be explained by the fact that when inversion relaxation is much slower than the round-trip time, a steady dynamic regime is possible only if the inversion changes little under the action of the generated pulse; in the two-section laser geometry, this inevitably results in small oscillations of the inversion near zero.

Next, we consider a case that is more important from a practical standpoint — the case of identical media in both laser sections, which implies equal transition dipole moments in the amplifier and the absorber. Indeed, selecting different media for the amplifier and absorber with a specified ratio of transition dipole moments, for example equal to two, appears to be a rather difficult task. In this regard, using the same medium in each laser section is much more convenient for practical implementation of the CML

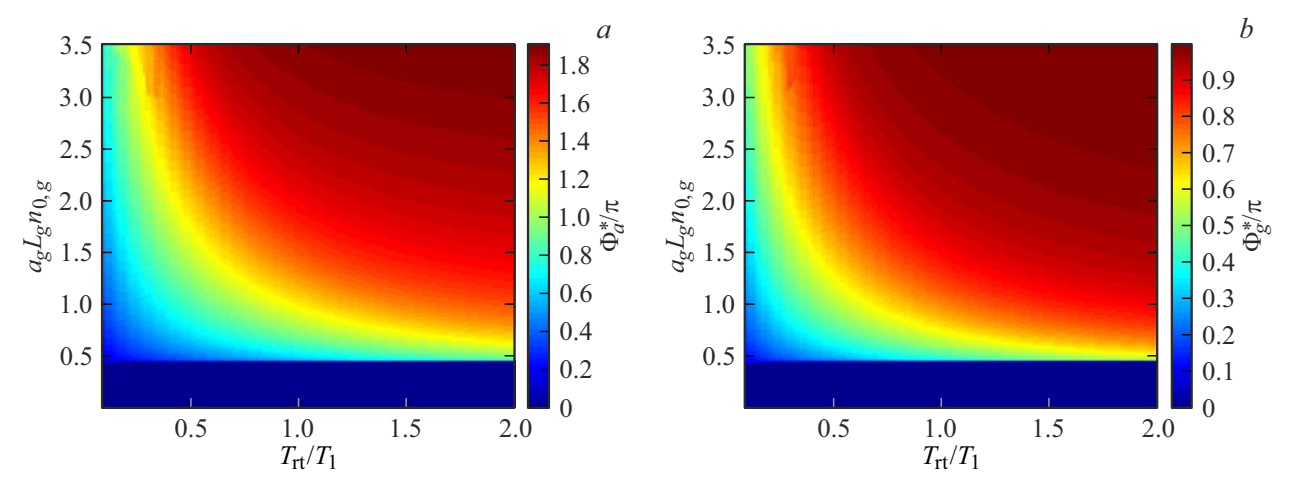


Figure 6. Steady-state pulse area at the output of the (a) absorber section Φ_a^* $(z=L_a)$, (b) amplifier section Φ_g^* $(z=L_g)$ as functions of the pump level $\alpha_g n_{0,g} L_g$ and the ratio of characteristic times $T_{\rm rt}/T_1$; other parameters: r=0.8, $T_{\rm rt}/T_2=2.5$, $m_d=2$, $\alpha_g n_{0,g} L_g=2\alpha_a n_{0,a} L_a$.

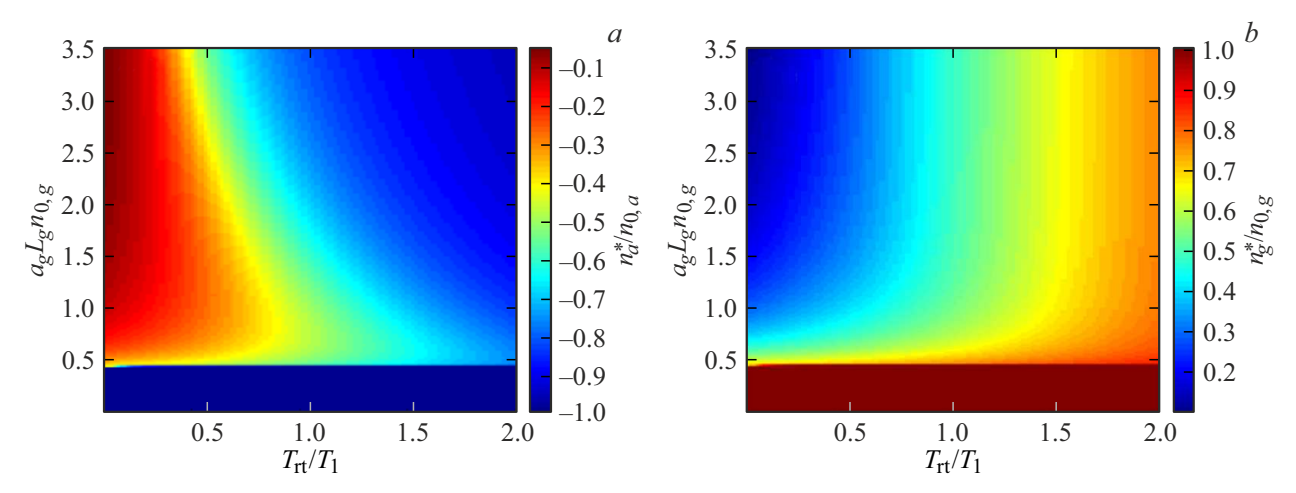


Figure 7. Steady-state population inversion at the output of the (a) absorber section n_a^* $(z = L_a)$, (b) amplifier section n_g^* $(z = L_g)$ as functions of the pump level $\alpha_g n_{0,g} L_g$ and the ratio of characteristic times $T_{\rm rt}/T_1$; other parameters: r = 0.8, $T_{\rm rt}/T_2 = 2.5$, $m_d = 2$, $\alpha_g n_{0,g} L_g = 2\alpha_a n_{0,a} L_a$.

regime. Figures 8, a and 8, b show the steady-state pulse area values at the output of the absorber and amplifier sections, respectively, for the case of identical media in both laser sections. In this case, the steady-state pulse areas do not exceed the value π in either section. Meanwhile, the pulse area in the amplifier tends toward the value π in the limit of high pumping and fast population inversion relaxation $T_{\rm rt}/T_1\gg 1$. At the same time, in the absorber, the pulse area monotonically decreases as the pulse propagates, and its steady-state values remain several times smaller than π over the whole parameter range. It is also noteworthy that the dependence of the steady-state pulse area in the absorber on the pump level shown in Fig. 8 a is non-monotonic: with increasing pump power, it first reaches a maximum and then gradually decreases.

Corresponding steady-state population inversion values in the absorber and amplifier for the case of the same medium in both laser sections are shown in Figs. 9, a and 9, b. Qualitatively, the shape of these diagrams resembles those in Figs. 7, a, b for the case of dipole moment ratio $m_d = 2$. However, for identical media in both amplifier and absorber, even with very fast population inversion relaxation, the steady-state inversion values are significantly lower than the equilibrium values $n_{0,g}$ and $n_{0,a}$. This is because, with equal dipole moments, the stable pulse area values in the gain and absorber media differ significantly.

Finally, we consider the case of an arbitrary ratio of the resonant transition dipole moments in the absorber and amplifier m_d . The diagrams in Figs. 9 and 10 show the steady-state pulse area values at the output of the absorber and amplifier as functions of the amplifier pump level and parameter m_d for fixed values of the ratios of characteristic times $T_{\rm rt}/T_1$ and $T_{\rm rt}/T_2$. For example, the diagrams in Fig. 6 a and 8, a for the absorber, corresponding to particular cases $m_d=1$ and $m_d=2$, and the diagram in Fig. 10(a) correspond to each other for identical values of the varied

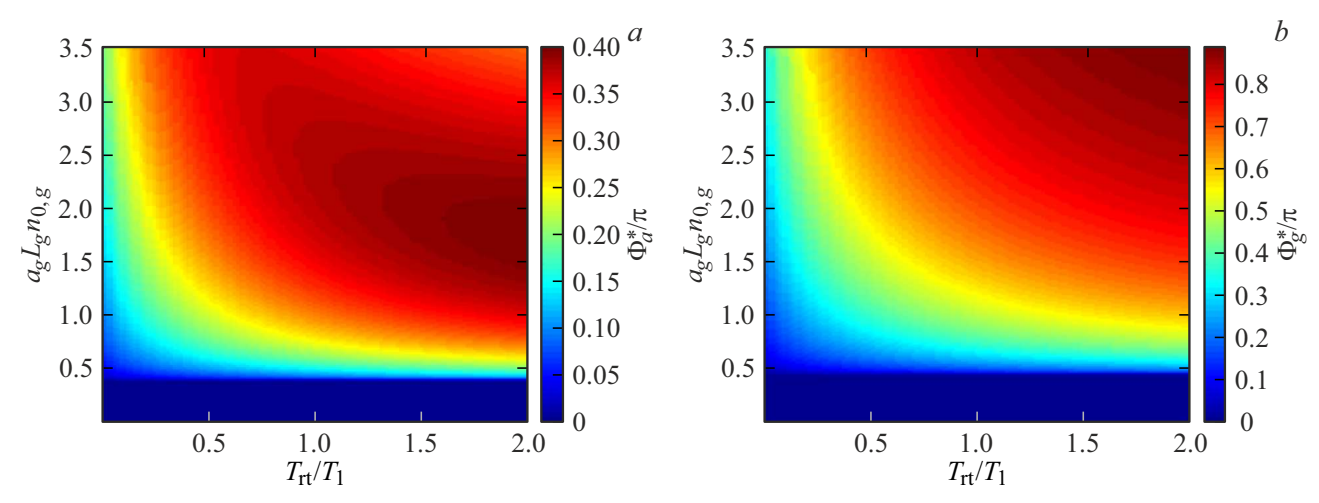


Figure 8. Steady-state pulse area at the output of the (a) absorber section Φ_a^* ($z = L_a$), (b) amplifier section Φ_g^* ($z = L_g$) as functions of the pump level $\alpha_g n_{0,g} L_g$ and ratio of characteristic times $T_{\rm rt}/T_1$; other parameters: r = 0.8, $T_{\rm rt}/T_2 = 2.5$, $m_d = 1$, $\alpha_g n_{0,g} L_g = 2\alpha_a n_{0,a} L_a$.

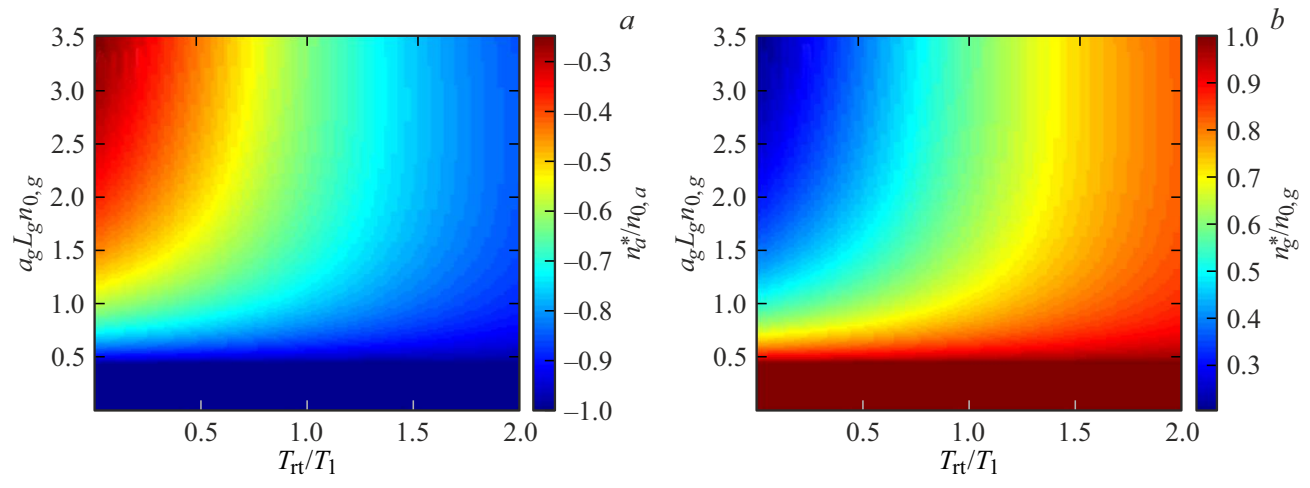


Figure 9. Steady-state population inversion at the output of the (a) absorber section n_a^* $(z=L_a)$, (b) amplifier section n_g^* $(z=L_g)$ as functions of the pump level $\alpha_g n_{0,g} L_g$ and the ratio of characteristic times $T_{\rm rt}/T_1$; other parameters: r=0.8, $T_{\rm rt}/T_2=2.5$, $m_d=1$, $\alpha_g n_{0,g} L_g=2\alpha_a n_{0,a} L_a$.

parameters. Specifically, a vertical cross-section at a given m_d in Fig. 10, a coincides with vertical cross-sections at $T_{\rm rt}/T_1=1$ in Fig. 6, a and 8, a.

As can be seen from the comparison of Figs. 10, a and 10, b, the dynamics of pulse area change in the steady-state CML regime differ significantly between the amplifying and absorbing media. Such differences seem natural given that the equilibrium pulse area values in infinitely extended media are different and equal to π in the amplifier and either 0 or 2π in the absorber. Fig. 10, a shows that the pulse area in the absorber remains below π in the steady generation regime for values of m_d up to ≈ 1.3 . For larger values of m_d the steady-state pulse area becomes greater than π and tends toward 2π in the limit of high pumping values. Furthermore, the pulse area reaches 2π most rapidly not near the optimal ratio $m_d = 2$, but rather at $m_d = 3$ because, in the range $2\pi < \Phi_0 < 3\pi$ the pulse

area during propagation in the absorber also tends to 2π . Meanwhile, the pulse area in the amplifier, as shown in Fig. 10, b, approaches the equilibrium value π near the optimal dipole moment ratio $m_d = 2$ whereas moving away from this value m_d in either direction causes the steady pulse area to decrease and deviate from π .

Steady-state population inversion values in the absorber and amplifier depending on the dipole moment ratio m_d are shown in Figs. 11, a, b. From Fig. 11, a it follows that the inversion in the absorber tends to its equilibrium value $-n_{0,a}$ both in the limit of very small $m_d \ll 1$, values (when, according to Fig. 10, a, the steady pulse area is close to zero) and near $m_d = 3$,when, according to Fig. 10, \dot{a} , the steady pulse area approaches 2π . Between these limits, the inversion in the absorber reaches a maximum around $-0.5n_{0,a}$. The population inversion in the amplifier section changes monotonically as m_d varies

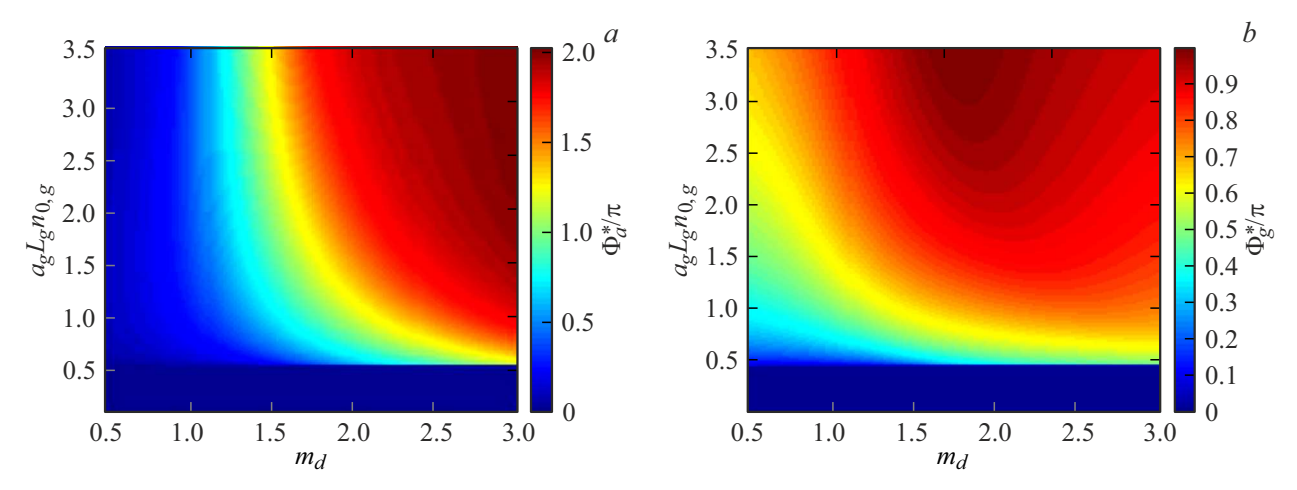


Figure 10. Steady-state pulse area at the output of the (a) absorber section Φ_a^* $(z = L_a)$, (b) amplifier section Φ_g^* $(z = L_g)$ as functions of the pump level $\alpha_g n_{0,g} L_g$ and the ratio of transition dipole moments in absorber and amplifier md; other parameters: r = 0.8, $T_{\rm rt}/T_1 = 1$, $T_{\rm rt}/T_2 = 2.5$, $\alpha_g n_{0,g} L_g = 2\alpha_a n_{0,a} L_a$.

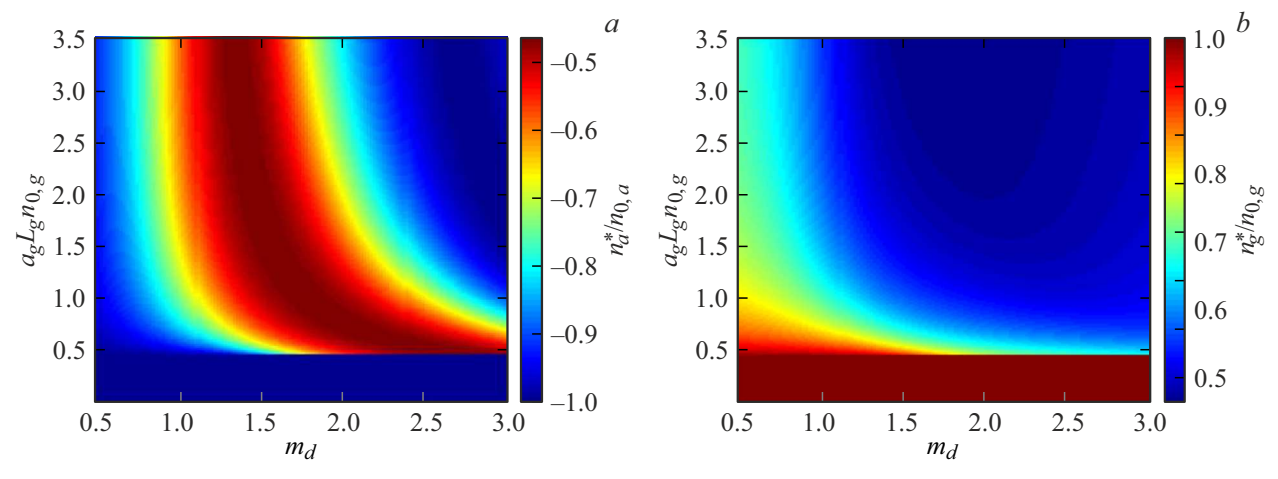


Figure 11. Steady-state population inversion at the output of the (a) absorber section n_a^* $(z = L_a)$, (b) amplifier section n_g^* $(z = L_g)$ as functions of pump level $\alpha_g n_{0,g} L_g$ and ratio of transition dipole moments in absorber and amplifier m_d ; other parameters: r = 0.8, $T_{\rm rl}/T_1 = 1$, $T_{\rm rl}/T_2 = 2.5$, $\alpha_g n_{0,g} L_g = 2\alpha_a n_{0,a} L_a$.

as shown in Fig. 11, b. Over the entire considered parameter range, inversion in the amplifier remains far from its equilibrium value $n_{0,g}$ due to the used relaxation time ratio $T_{\rm rt}/T_1=1$, implying relatively slow inversion relaxation in the amplifier over one resonator round-trip. The equilibrium population inversion in this case decreases with both increasing pump level and the parameter m_d .

Conclusion

A comprehensive analytical and numerical study was conducted on the influence of the parameters of the amplifying and absorbing media on the coherent mode locking dynamics in a two-section laser with parameters typical for quantum cascade lasers. It was found that the ratio of relaxation times T_2/T_1 is a critical parameter

determining generation characteristics; in particular, the polarization relaxation time T_2 may vary with changes in device temperature. It was shown that within the range $0.1 < T_2/T_1 < 0.6$ increasing T_2 leads to increased pulse power accompanied by pulse shortening, with generation regime stability maintained. The results of investigating the influence of the ratio of dipole moments in the absorber and amplifier d_a/d_g : are also of interest: for $d_g = 7D$ varying the absorber dipole moment d_a results in complex dynamics with switching between multi-pulse regimes, while for $d_g = 5D$ a stable operating range $1.2 < d_a/d_g < 3$ was found where the pulse amplitude triples and pulse duration shortens to 160 fs with stable generation maintained. Since the dipole moment of the radiative transition in QCL depends on the applied electric field, this allows changing the generation parameters without replacing the resonator section.

The application of the analytical approach based on the generalized area theorem confirmed the stability of the CML regime above the pump threshold and allowed identifying optimal parameters for efficient energy exchange in the system. The obtained results are important for developing compact short-pulse sources based on quantum cascade lasers in the IR and THz ranges and open new opportunities for controlling generation parameters in such systems.

Funding

This research was supported financially by the Foundation for the Advancement of Theoretical Physics and Mathematics "BASIS" (analytical and numerical calculations) and the State task of the A.F. Ioffe Physical-Technical Institute, 0040-2019-0017 (analysis of the results).

Conflict of interest

The authors of this paper declare that they have no conflict of interest.

References

- [1] V.V. Kozlov. Phys. Rev. A, 56, 1607 (1997).
- [2] S.L. McCall, E.L. Hahn. Phys. Rev., **183**, 457 (1969).
- [3] L. Allen, J.H. Eberly. Optical resonance and two-level atoms (Wiley, N. Y., 1975).
- [4] M.A. Talukder, C.R. Menyuk. Phys. Rev. A, 79, 063841 (2009).
- [5] R. Arkhipov, M. Arkhipov, I. Babushkin. Opt. Commun., 361, 73 (2016).
- [6] R.M. Arkhipov, M.V. Arkhipov, I. Babushkin, N.N. Rosanov. Opt. Lett., 41, 737 (2016).
- [7] R. Arkhipov, M. Arkhipov, A. Pakhomov, I. Babushkin, N. Rosanov. Phys. Rev. A, 105, 013526 (2022).
- [8] A. Outafat, S. Faci, E. Richalot, S. Protat, C. Algani. Opt. Quant. Electron., 54 (5), 283 (2022).
- [9] U. Keller. Appl. Phys. B, **100**, 15 (2010).
- [10] J.C. Diels, W. Rudolph. *Ultrashort laser pulse phenomena* (Elsevier, 2006).
- [11] A. Pakhomov, M. Arkhipov, N. Rosanov, R. Arkhipov. Phys. Rev. A, 108, 023506 (2023).
- [12] A. Pakhomov, R. Arkhipov. Phys. Rev. A, 109, 033519 (2024).
- [13] M.V. Arkhipov, A.A. Shimko, N.N. Rosanov, I. Babushkin, R.M. Arkhipov. Phys. Rev. A, 101 (1), 013803 (2020).
- [14] R. Paiella, F. Capasso, C. Gmachl, D.L. Sivco, J.N. Baillargeon, A.L. Hutchinson, A.Y. Cho, H.C. Liu. Science, 290, 1739–1742 (2000).
- [15] R. Paiella, F. Capasso, C. Gmachl, H.Y. Hwang, D.L. Sivco, A.L. Hutchinson, A.Y. Cho, H.C. Liu. Appl. Phys. Lett., 77, 169-171 (2000).
- [16] C.Y. Wang, L. Kuznetsova, V.M. Gkortsas, L. Diehl, F.X. Kärtner, M.A. Belkin, A. Belyanin, X. Li, D. Ham, H. Schneider, P. Grant, C.Y. Song, S. Haffouz, Z.R. Wasilewski, H.C. Liu, F. Capasso. Opt. Express, 17, 12929–12943 (2009).
- [17] M.A. Talukder, C.R. Menyuk. Optics Express, 22 (13), 15608-15617 (2014).

- [18] E. Riccardi, V. Pistore, S. Kang, L. Seitner, A. De Vetter, C. Jirauschek, J. Mangeney, L. Li, A.G. Davies, E.H. Linfeld et al. Nat. Photon., 17, 1–8 (2023).
- [19] R.M. Arkhipov, M.V. Arkhipov, O.O. Diachkova, A.V. Pakhomov, N.N. Rosanov. Opt. Spectrosc., 131 (7), 884(2023).
- [20] R. Arkhipov, O. Diachkova, A. Pakhomov, M. Arkhipov, N. Rosanov, B. Zhmud, R. Khabibullin. Appl. Phys. B, 130 (10), 184 (2024).
- [21] H. Choi, V.M. Gkortsas, L. Diehl, D. Bour, S. Corzine, J. Zhu, G. Höfler, F. Capasso, F.X. Kärtner, T.B. Norris. Nature Photonics, 4, 706 (2010).

Translated by J.Savelyeva